Proceedings of ASME Turbomachinery Technical Conference & Exposition
GT2019
June 17-21, 2019, Phoenix, AZ, USA

GT2019-91095

ROLE OF TURBULENCE IN PRECESSING VORTEX CORE DYNAMICS

Ashwini Karmarkar, Mark Frederick, Sean Clees, Danielle Mason, Jacqueline O'Connor
Pennsylvania State University
University Park, PA 16802

ABSTRACT

Precessing vortex cores (PVC), arising from a global instability in swirling flows, can dramatically alter the dynamics of swirl-stabilized flames. Previous study of these instabilities has identified their frequencies and potential for interaction with the shear layer instabilities also present in swirling flows. In this work, we investigate the dynamics of precessing vortex cores at a range of swirl numbers and the impact that turbulence, which tends to increase with swirl number due to the increase in mean shear, has on the dynamics of this instability. This is particularly interesting as stability predictions have previously incorporated turbulence effects using an eddy viscosity model, which only captures the impact of turbulence on the base flow, not on the instantaneous dynamics of the PVC itself. Time-resolved experimental measurements of the three-component velocity field at ten swirl numbers show that at lower swirl numbers, the PVC is affected by turbulence through the presence of vortex jitter. With increasing swirl number, the PVC jitter decreases as the PVC strength increases. There is a critical swirl number below which jitter of the PVC vortex monotonically increases with increasing swirl number, and beyond which the jitter decreases, indicating that the strength of the PVC dominates over turbulent fluctuations at higher swirl numbers, despite the fact that the turbulence intensities continue to rise with increasing swirl number. Further, we use a nonlinear van der Pol oscillator model to explain the competition between the random turbulent fluctuations and coherent oscillations of the PVC. The results of this work indicate that while both the strength of the PVC and magnitude of turbulence intensity increase with increasing swirl number, there are defined regimes where each of them hold a stronger influence on the large-scale, coherent dynamics of the flow field.

NOMENCLATURE

A	Amplitude of harmonic forcing function
D	Nozzle diameter
R_{rms}	Root mean square value of the radial coordinate at regular phase intervals
S	Geometric swirl number
X_{rms}	Root mean square value of the axial coordinate at regular phase intervals
f	Frequency
f_r	Resonant frequency of the noise forced van der Pol oscillator
r	Radial coordinate
t	Time
u'_{rms}	Net turbulence intensity at a single location
x	Axial coordinate
μ	Nonlinearity parameter in van der Pol oscillator
ω	Vorticity
σ	Amplitude of white Gaussian noise
θ	Swirler blade angle
wgn	White Gaussian noise

INTRODUCTION

Swirling flows are commonly used for enhancing flame stability in gas turbine combustors. The property that makes them suited for this application is a phenomenon known as vortex breakdown [1–9], characterized by the formation of an central recirculation zone (also known as the vortex breakdown bubble) that constantly supplies hot gases and active radicals to the base of the flame, enhancing its static stability. This recirculation zone is created when the degree of swirl exceeds a certain critical num-

ber and the pressure gradient along the axis is too large to be balanced by axial flow. In combustors, the occurrence of this breakdown bubble depends largely on the swirl number and the combustor configuration, particularly the dump ratio (ratio of the combustor area to the nozzle area) and the exit boundary condition.

With increasing swirl, there comes a point when this vortex bubble becomes unstable and periodically precesses about the central axis of the flow, forming the precessing vortex core (PVC). PVCs are a self-excited global instability that lead to large-scale helical disturbances in the flow field [10–12]. In combustor systems, the occurrence of a PVC is a function of swirl number, flame shape, fuel/air mixing, combustor configuration, and equivalence ratio [13]. Oberleithner *et al*. [14] showed that the formation of the PVC depends on the density and temperature gradient near the combustor inlet. Freitag *et al*. [15] showed that the PVCs significantly enhance fuel air mixing. Steinberg *et al*. [16] showed that in some cases, the PVC can couple with thermoacoustic fluctuations.

Previous work from our group has shown, through a spectral analysis of the flow, that response of the shear layers to acoustic forcing can be suppressed in the presence of a PVC [17]. This result has been explained by means of a linear stability analysis, showing that the formation of the PVC results in increased shear layer thickness. This increased thickness leads to a progressive weakening of the Kevin Helmholtz mechanism that ultimately causes reduced shear layer receptivity [18]. This result was shown experimentally for a moderate range of forcing frequencies and amplitudes, but more thoroughly in the linear stability analysis over almost two orders of magnitude in forcing frequency. The implications for this result are important to the prediction of thermoacoustic instability in combustion systems. As velocity coupling, where heat release rate oscillations are driven by velocity oscillations in the flow field, is a major contributor to the thermoacoustic feedback loop, the suppression of coherent vortical velocity fluctuations that modulate the flame at the acoustic frequency can be a direct method of suppressing combustion instability. To achieve this goal, however, accurate prediction of the dynamics of the PVC must be achieved at realistic combustor conditions, which include high turbulence intensities.

Several methods have been used to extract coherent structures like the PVC from a turbulent flow field. Most of these techniques rely on a triple decomposition, proposed by Hussain and Reynolds [19], which is a method based on the premise that every instantaneous signal can be decomposed into the mean value, a coherent component, and random oscillations. They originally used phase averaging to extract the coherent structures. This method, however, requires knowledge of the cycle period and neglects any information about cycle to cycle variation of the coherent oscillation, or 'jitter.' Midgley *et al*. [20] used conditional averaging of the Reynolds-decomposed velocity field to separate 'true' turbulence and large-scale structures. Some approaches have used frequency domain filtering. For instance, Liou and Santavicca [21] used a low pass digital filter and Brereton and Kodal [22] proposed a method to estimate the power spectral densities of the data to yield an optimized frequency domain filter. Proper orthogonal decomposition (POD) and has been used to isolate coherent structures [23–28]. Hydrodynamic stability analyses [23, 28] have also been used to isolate large scale instabilities.

The goal of this study is to characterize the influence of turbulence on PVC dynamics and identify flow regimes where this influence alters the PVC dynamics. We make this characterization by quantifying the jitter of the coherent structures that arise from the PVC instability, where jitter is the cycle to cycle variation in the behavior of the coherent structures [29]. Our hypothesis is that PVC jitter is a result of the influence of turbulent motions on the PVC structures, where the amplitude of the jiter is determined by the relative magnitude of the turbulent oscillations versus the strength of the PVC oscillator. If that is the case, the magnitude of jitter could be used to quantify the degree of influence that turbulence has on the PVC.

We observe the variation in PVC motion with increasing swirl number and quantify jitter in both space and time. We also analyze the behaviour of a nonlinear oscillator in a model problem to explain the experimental results we observe. The behavior of this model oscillator provides insight into the dynamics of a nonlinear system that is driven by both coherent and random oscillations and the regimes where each of these oscillations dominates the system. The analogy between the behavior of this oscillator and the flow field dynamics of our system allows us to interpret the variation in jitter with swirl number.

The results of this study are pertinent to our previous work in two ways. First, understanding the role of turbulence in the behavior of coherent oscillations is an important step towards improving theoretical predictions of flow instabilities. While turbulence is now regularly accounted for in the structure of the base flow through an eddy viscosity model, current predictions do not account for turbulence on the instantaneous dynamics of the PVC. This study seeks to understand if this omission is critical or not to predicting the PVC dynamics. Second, our previous results showed that the PVC could suppress the receptivity of the shear layers to external perturbations. This method was previously proposed as a way of suppressing thermoacoustic oscillations in combustors, as the velocity-coupled flame response would be suppressed if there was no shear layer response to acoustic oscillations. Utilizing this method of thermoacoustic suppression, however, requires better knowledge of the instantaneous PVC dynamics in realistic combustor flows, which typically have very high turbulence intensities. Whether or not the PVC plays a critical dynamical role as turbulence increases is still an open question, and one we begin to answer with the present study.

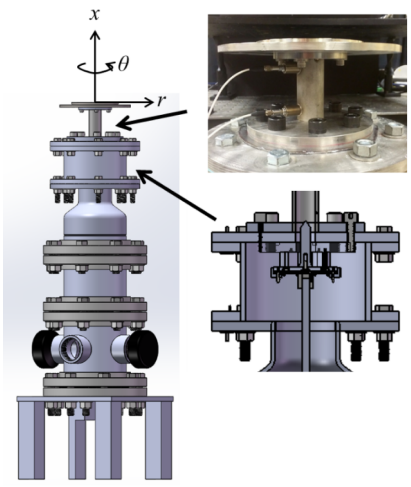

FIGURE 1. Experimental configuration.

METHODS

Experimental Configuration

The experiment was conducted in the swirling jet experiment shown in Fig. 1. The swirler blade angle is varied using an encoded stepper motor in increments of 2.5° to provide a variation in the degree of swirl without changing the flow rate. The swirler consists of eight evenly spaced NACA 0025 airfoils of height 1 in. and chord length of 1 in. The swirler blade angles can range from $-70°$ to 70°. As the blade angle varies, the blockage increases, which alters the pressure drop and acoustic impedance of the swirler [17]; given that the experiment operates at atmospheric pressure, we do not expect this change in swirler blockage to dramatically alter the flow velocity.

The setup shown in Fig. 1 includes the following components: the injector nozzle with two pressure transducers (top right), the variable angle swirling chamber, the radial entry swirler (bottom right), and the settling chamber. There is a 1 in. inlet port at the bottom of the rig through which room-temperature air enters; flow is metered using a thermal mass flow meter (Teledyne Hastings), which has a 0.5% flow rate uncertainty. In all cases tested, the flow rate remained within 0.12% of the 953.0 SLPM set point, resulting in a bulk velocity of 28 m/s from the nozzle. The air then travels into the settling chamber, which has perforated plates at each end to break up any large flow structures. The flow then passes through a smooth contraction, going from 6 in. to 3 in. in diameter, which guides the flow to create a radially uniform velocity profile before it enters the swirler. The air exits the swirler axially and encounters two pressure transducers before it exits to the atmosphere through a 1 in. diameter nozzle.

Diagnostics

The pressure transducers (PT) are located 2.54 cm and 7.62 cm downstream of the swirler, which is 6.92 cm and 1.84 cm from the nozzle exit, respectively. A Hawk/Darwin Duo Nd-YAG, 532 nm wavelength, 60 W laser is used for measuring three components of velocity using particle image velocimetry (PIV). For all cases, the laser is directed through a 50 mm sheet optic to produce a laser sheet in the $x-r$ plane; the referenced coordinate system is depicted in Fig. 1.

Velocity fields were captured using stereoscopic PIV with images from two SA5 Photron complementary metal oxide semiconductor (CMOS) high speed cameras. The sampling rate of the PIV system is 5 kHz, with an interframe time ranging from 22 to 24 s depending on swirl number. The coherent structures in the flow oscillate at frequencies less than 1 kHz, and so the 5 kHz data acquisition rate is suitable for capturing these oscillations. Images were recorded for a one second duration, yielding 5000 frames per test case. The PIV system is triggered simultaneously with the PTs. Aluminum oxide particles with a nominal diameter of 12 m were used as tracer particles and can accurately follow flow perturbations up to a frequency of 4000 Hz. Velocity vectors were calculated in DaVis 8.3.1 without any pre-processing or masking of the images.

To calculate the velocity vectors, cross-correlation with multi-pass iterations with decreasing window sizes is used. The first pass is a 32x32 pixel interrogation window with a 50% overlap followed by two passes with a 16x16 pixel interrogation with a 50% overlap. During vector post-processing, two methods were used to reject vectors. First, if the vector is more than three times the RMS of the surrounding vectors, the vector is replaced. Additionally, universal outlier detection replaces spurious vector results. Uncertainty calculations on the mean vector field for each test case did not exceed 2 m/s.

Analysis

The jitter in the spatiotemporal evolution of the PVC is quantified in two different ways. As the PVC oscillations manifest in disturbances that develop in both space and time, jitter in the PVC oscillations will manifest as both "spatial jitter," or the variation of the spatial location of the PVC at a given phase of the oscillation, and "frequency jitter," or the variation of the frequency of the PVC oscillation. The connection between these two metrics of the jitter can be understood by considering the actual structure of the precessing vortex core, which is where the vortex breakdown bubble orbits (or precesses) around the geometric center of the jet [13]. If the circumference of this precession changes due to turbulent oscillations, then the location of the PVC-induced vortices in *space* will vary (the manifestation of "spatial jitter"). Additionally, if that precession circumference changes, then the *time* it takes to precess will vary, which manifests as a change in the frequency of PVC oscillation (or

"frequency jitter"). As such, the spatial and frequency jitter are manifestations of the same process, and we can quantify the jitter of the PVC in both ways.

To quantify the phase jitter of the PVC motion, we first filter the flow field and then use phase-averaging to identify the PVC vortices in each period of the PVC oscillation, essentially performing a triple decomposition. To filter the flow field, we perform a proper orthogonal decomposition on the three-component velocity field and extract the PVC modes. PVC modes are identified in two ways. First, they are the most energetic modes in the flow. Second, we determine which of the high-energy modes are PVC modes by inspecting the spatial mode shapes of the radial velocity component. From here, the typical PVC shape can be identified, as can be seen in Fig. 6. The high energy modes are reconstructed into a time series to obtain the velocity vectors for coherent motion alone. The sensitivity of the jitter calculation to this filtering process is tested by varying the number of modes that are included in the POD reconstruction. The number of modes included is systematically varied, and it is seen that the response stabilizes after a certain number. We present results of the POD filtering at this cut-off.

This POD-filtered time series is used to track the PVC vortices during each period of the PVC oscillation, providing information about the spatial jitter of the PVC. The filtering process does not eliminate the effect of turbulence on the PVC, as this is a nonlinear interaction and inherently "built in" to the PVC modes; eliminating the remaining modes simply reduces the noise on top of the PVC motion. To identify the jitter of the PVC location, we perform a phase-resolved extraction of the vortex location. The vortex is identified from the instantaneous, POD-filtered vorticity field by identifying local peaks in vorticity. We use this criterion because in cases with no wall shear, it is an accurate method of identifying vortices [30]. We then calculate the time period of vortex shedding using the instability frequency obtained from POD. The identified vortex is then tracked through time and its locations at a given phase are stored. In case the time period calculated from the instability frequency is not a multiple of the time step of the measurement, a linear interpolation is performed between the vortex location in the time step immediately before and the time step immediately after the required time. Once this is done for the complete data set corresponding to a single swirl number, we calculate the RMS of all the axial and radial locations corresponding to the same geometric phase. This RMS value is used as a metric to represent the magnitude of spatial jitter. This procedure is repeated for the first PVC vortex at every swirl number. The geometric swirl number is calculated using the expression $S = \frac{2}{3}\tan\theta$, where θ is the swirler blade angle [31].

In order to observe the variation in the turbulence intensity, all the POD modes except the high energy modes (corresponding to the PVC) are reconstructed to obtain a time series of three-component velocity vectors. The resulting time series represents the random turbulent component of the triple decomposition. The turbulence intensity is calculated at the mean vortex location using this reconstructed velocity field for every swirl number.

To quantify the temporal jitter of the PVC, we perform a spectral proper orthogonal decomposition (SPOD) on the velocity data to obtain the frequency spectra of the most energetic modes, which represent the PVC. The SPOD method is taken from Towne *et al*. [26] and the PVC modes are identified using the same metrics as in the POD filtering above, by observing the spatial mode shape of the radial velocity fluctuations. As SPOD provides a frequency-resolved decomposition, the PVC can be uniquely identified in both frequency and energy space. In energy space, it is evident that the first mode contains almost the entirety ($> 95\%$) of the PVC motion; as such, we only consider the spectra of Mode 1 for PVC identification. In spectral space (of Mode 1), we quantify the temporal jitter of the PVC using the width of the peak around the PVC frequency.

We use SPOD to quantify frequency jitter rather than using a snapshot POD method, which provides spatially-orthogonal, energy-ordered modes of the dataset, because POD does not discern motions based on their spatiotemporal evolution, just their spatial correlations. As a result, tonal but spatially un-correlated or low-energy oscillations are not necessarily separated from other motions in the POD, but can be identified in the SPOD. SPOD achieves this by calculating the eigenvalue problem on the cross-spectral density tensor, which results in spatial modes analogous to this from snapshot POD, but also provides frequency-resolved energy information about each of these modes. Towne *et al.* [26] rigorously show that SPOD is an optimized dynamic mode decomposition (DMD) [32] method for stationary flows; discussion of this relationship is beyond the scope of this paper, but is the reason that we do not use DMD.

RESULTS

The time-averaged flow profiles for a range of swirl numbers have previously been discussed by Frederick *et al*. [18] and are shown in Fig. 2. Pre-vortex breakdown swirling jets correspond to $0 \leq S \leq 0.38$, before a recirculation zone forms. Intermittent vortex breakdown occurs when $0.38 < S \leq 0.56$ and is characterized by highly intermittent behavior along the centerline. Analysis in this paper begins with steady vortex breakdown, classified by a time-averaged recirculation along the centerline, for which $0.56 < S \leq 0.67$. In Fig. 2, the contours clearly show a decrease in axial velocity along the centerline as S increases from 0.61 to 0.67. For $0.67 < S \leq 0.87$, the flow field is in the weak PVC state. A PVC is characterized by a narrow-band frequency and in the weak PVC state, this defining frequency shows intermittency. For all $S \geq 0.95$, the flow field is characterized by a strong PVC. The cases considered in this study all have relatively high swirl numbers, where there is continuous recirculation along the cen-

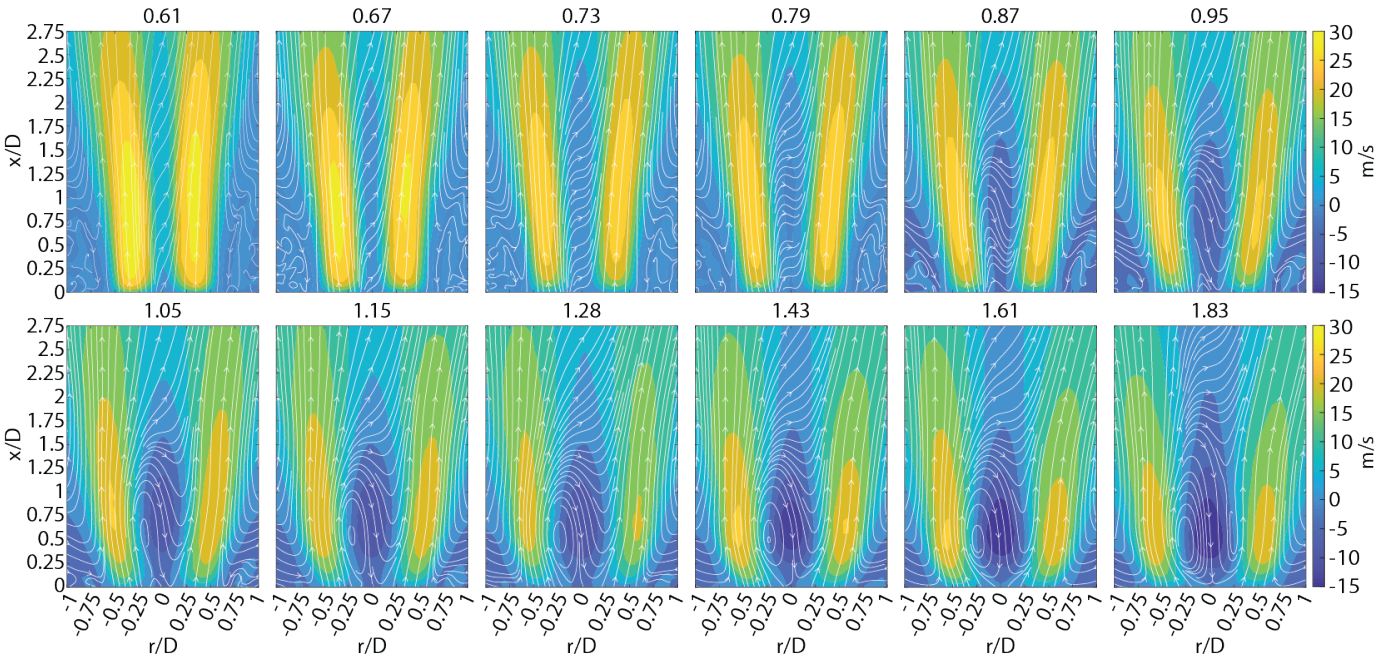

FIGURE 2. Time-averaged axial velocity contours and streamlines at a range of swirl numbers.

terline (in the vortex breakdown bubble) and the PVC is present in all cases.

The frequency and amplitude of the PVC as a function of swirl number is shown in Fig. 3; these measurements are taken from the pressure transducer closest to the nozzle exit. As the swirl number increases, both the frequency and amplitude of PVC oscillations increases monotonically. The bars on the frequency represent the full-width, half-max of the spectral peak at the PVC frequency from the pressure data. Additionally, the pressure transducers do not register the weak oscillations of the PVC at swirl numbers less than $S = 0.95$, and so no data is provided there. However, the PVC is visible in the velocity data at these lower swirl numbers, as will be discussed in the next sections.

To study the motion of the PVC, we perform proper orthogonal decomposition on the velocity data. POD gives us the eigenmodes of the data matrix, ranked in order of decreasing modal energy. The modes with the highest energies represent the large scale coherent fluctuations in the flow field and the lower energy modes represent random oscillations or turbulence. We reconstruct the velocity vectors of these high energy modes to extract the flow field describing the motion of the PVC. Since the PVC is a harmonically oscillating structure, the influence of the surrounding turbulence is largely responsible for any significant deviation from its coherent behaviour. This disruption of coherent behaviour can be characterized by measurement of the cycle to cycle variation in phase, or 'jitter.' The precession of the vortex

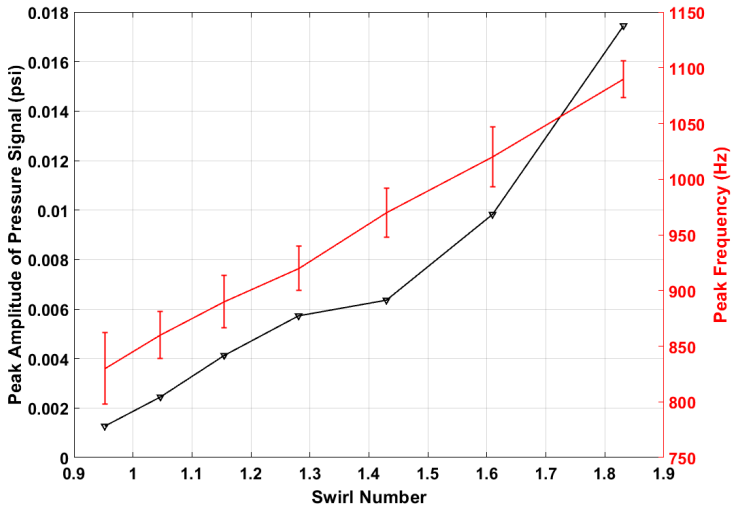

FIGURE 3. Variation in PVC frequency and amplitude (with error bars representing the peak width) obtained from pressure transducer data.

core is inherently a spatio-temporal phenomenon, which allows variation in jitter to be measured in both space and time domains. In this study, we observe jitter in both these domains, and offer a hypothesis to reconcile the results obtained.

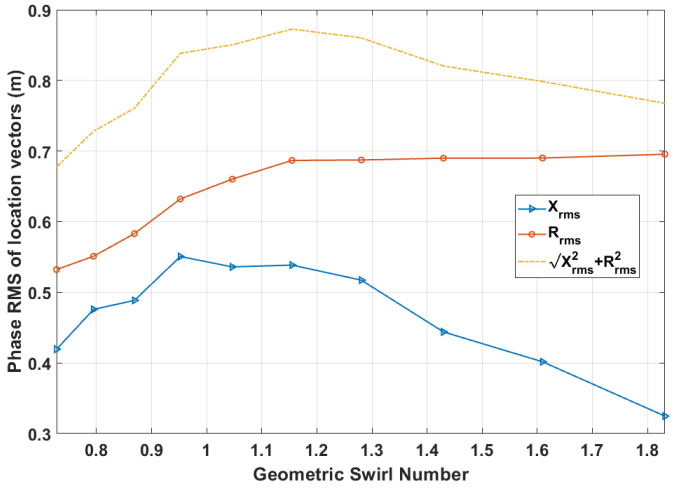

FIGURE 4. Variation in vortex location RMS with swirl number.

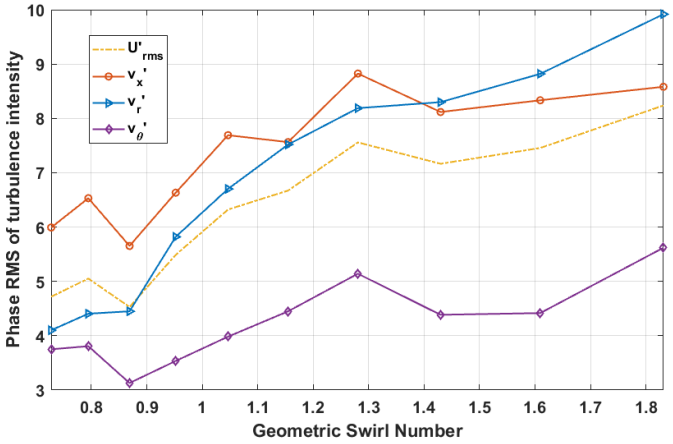

FIGURE 5. Variation in turbulence intensity at the mean vortex location with swirl number.

Spatial Characterization of Jitter

To spatially characterize jitter, we observe the motion of the vortices caused by the PVC at regular phase intervals and calculate the RMS of the vortex centroid in both the axial and radial directions, as shown in Fig. 4. Additionally, the turbulence level at the centroid of the vortex location is shown as a function of swirl number in Fig. 5. The turbulence intensity is calculated from a POD-filtered velocity field, which is comprised of all the modes that are not the PVC so that the change in PVC intensity does not bias the velocity RMS values.

From the plots, it can be seen that up to a swirl number of approximately $S = 1.1$, the magnitude of jitter increases, and after this critical value, the jitter reduces. While the RMS level in the radial position stabilizes above the critical swirl number, the RMS level in the axial position decreases, causing an overall drop in the amplitude of spatial jitter. In Fig. 4, this can be seen by the total RMS line (no symbols), which peaks at a swirl number of $S = 1.1$ and decreases with increasing swirl number. This drop occurs despite the increase in turbulence intensity at the location of the vortex, which increases continuously with swirl number. We perform the jitter calculation at varying phase intervals throughout the PVC cycle and the results show the same trends at all phases. Additionally, differences in the behavior of the radial and axial location RMS variations cannot be explained by variations in the components of the turbulent velocity fluctuations. Fig. 5 shows that all three velocity fluctuation components, as well as the total turbulence level, increases with swirl number with approximately the same slope. It was previously confirmed that turbulent statistics were converged [18].

Frequency Domain Characterization of Jitter

An alternate way of quantifying jitter is to consider the frequency jitter, which we determine using the peak width of the PVC frequency peak from the velocity field decomposition from SPOD. The radial mode shapes of the first mode for a select number of cases, shown in Fig. 6, are taken from the peak frequency of Mode 1 in the SPOD and correspond to the PVC. These mode shapes show that the PVC becomes more defined with increasing swirl number. It can also be seen that as the swirl number increases, the PVC structure moves towards the nozzle, a result of the vortex breakdown bubble shifting upstream. Additionally, the oscillation becomes spatially more compact, a result of the increasing frequency of the oscillation and the constant bulk flow velocity of each case. Figure 7 shows the frequency spectra of select swirl numbers for the first mode (or the highest energy mode), which is the mode that includes the dynamics of the precessing vortex core.

Because of the harmonic nature of the PVC, there is a peak at the PVC frequency and the width of the peak is a measure of the cycle to cycle variation in the frequency of oscillation, or 'frequency jitter.' Since the precession of the vortex core is a spatio-temporal phenomenon, the frequency jitter is inherently linked to the spatial jitter. As the precession orbit of the PVC varies in time (which registers as jitter in space), the frequency of the precession also varies and increases the width of the peak of the PVC in the spectrum. We use the velocity spectra from the SPOD since these spectra contain information about the entire flow field, rather than just one location in the flow field. We found that PVC amplitude and peak width could vary significantly if velocity time series were extracted from different spatial locations in the flow field, as the PVC oscillations are only located in certain parts of the flow field. To avoid any ambiguity regarding PVC location, the spectra from the SPOD are considered instead.

Fig. 8 shows the peak width (full-width, half-max) of the

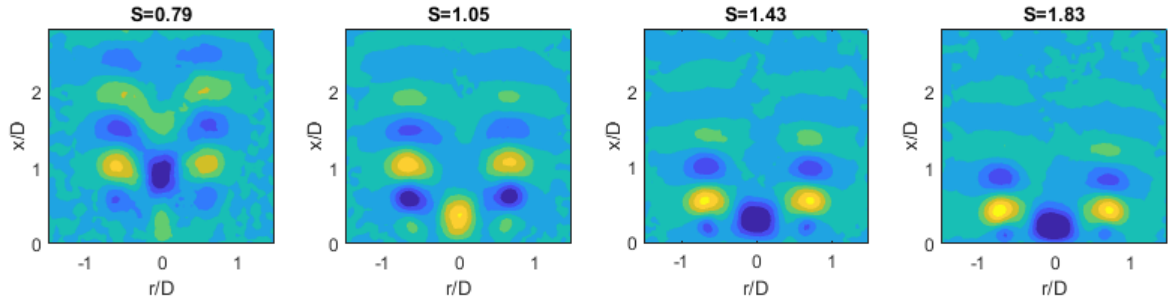

FIGURE 6. SPOD mode shapes of the first mode for select swirl numbers at their respective PVC frequencies.

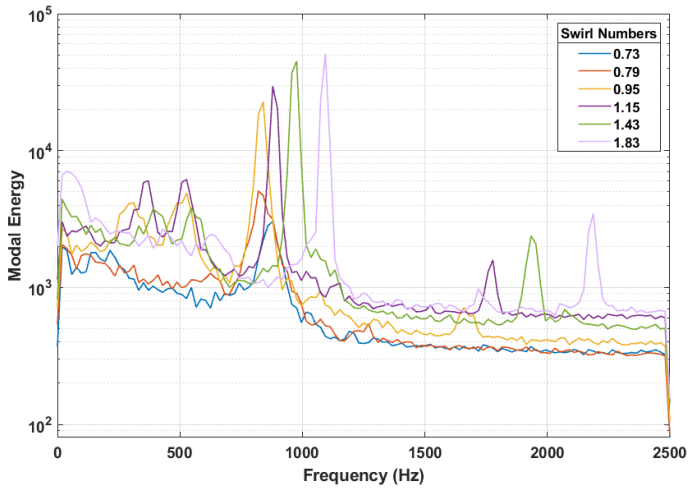

FIGURE 7. Modal energy spectra of the first SPOD mode.

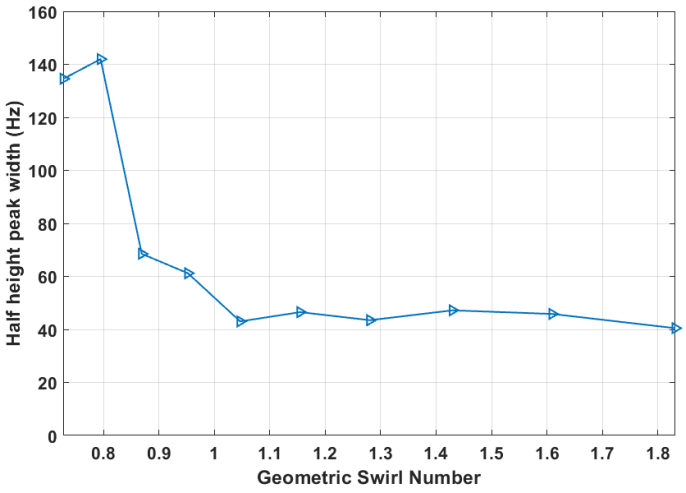

FIGURE 8. Peak width at half the peak height of the first SPOD mode frequency domain spectra.

SPOD spectra as a function of the swirl number. The peak width decreases as swirl number increases until approximately $S = 1.05$, after which the peak width is relatively constant with increasing swirl number. This trend indicates that beyond swirl number $S = 1.05$, the frequency jitter is no longer sensitive to increasing turbulence. The peak height, however, continues to increase, indicating that the PVC is getting stronger. For two specific cases, ($S = 1.15$ and $S = 1.28$), the peak height dips a little and smaller peaks at lower frequencies are visible; these lower frequency dynamics are intermittent and likely the result of oscillations in the swirler. They are also an order of magnitude lower in amplitude than the PVC peak, indicating that the PVC is still the most energetic feature in the flow field. To this point, at higher swirl numbers, the first harmonic of the PVC frequency is also visible in the spectrum, an indication of the nonlinear behavior of the oscillator at this very high amplitude. Overall, the trend that the peak width follows with increasing swirl number is very similar to the trend observed in the spatial jitter characterization, although the critical swirl number at which turbulence no longer causes increasing jitter is slightly lower.

DISCUSSION

To better understand the dynamics of the PVC in the presence of turbulence, we model the flow field dynamics as an interaction between two competing parameters: flow field turbulence and coherent PVC dynamics. As the swirl number increases, both the PVC amplitude as well as the turbulence intensity increase. The PVC amplitude increases due to the stronger central recirculation at higher swirl numbers, which results in an increase in shear along the inner shear layers; previous linear stability analysis has shown that increasing the mean shear in the inner shear layer results in larger growth rates of the instability that causes the PVC [33]. The turbulence levels increase with swirl number as a result of increasing mean shear in the flow field. To model this system, we use a nonlinear oscillator forced by noise and a coherent forcing function. Here, we consider a van der Pol oscillator [34] forced by white Gaussian noise and a

sinusoidal forcing function the resonant frequency of the oscillator. The noise is meant to mimic the turbulent fluctuations, while the sinusoidal forcing is meant to mimic the "wavemaker" that drives the PVC. The nonlinear differential equation governing this system is,

$$\frac{d^2y}{dt^2} - \mu(1-x^2)\frac{dy}{dt} + y = \sigma(wgn) + A\sin(2\pi f_r t)$$

where y is the operating variable, μ is the nonlinearity parameter, wgn is the white Gaussian noise function, and f_r is a frequency at the resonant frequency of the oscillator.

To understand the competing impact of random vs. coherent forcing on the nonlinear oscillator, we systematically vary the noise amplitude, σ, and the wavemaker amplitude, A, and calculate the RMS of the variable y to quantify the amplitude of the resulting oscillations, shown in Fig. 9. The nonlinearity parameter, μ is set to 0.5, although any value between 0 and 1 provides similar results. At lower values of harmonic amplitude, the response parameter, y_{rms} is very sensitive to noise, but with increasing harmonic amplitude, the sensitivity of y_{rms} to noise amplitude decreases. For example, when $\sigma = 0.1$, the y_{rms} levels are commiserate with the random forcing for low A, but then increase with increasing A at amplitudes $A > 1$. At higher noise levels, like $\sigma = 10$, the oscillator is "noise driven" for a wider range of A. However, in all cases, at high enough harmonic forcing, the y_{rms} trends collapse onto the $\sigma = 0$ line, indicating that despite the presence of random forcing, the increase in harmonic forcing drives the system oscillations at high levels of A, which would result in smaller levels of jitter from the random oscillations.

In the swirling flow system being considered, it is evident from Fig. 5 and Fig. 7 that while both turbulence and PVC strength are low for lower swirl numbers and both increase with increasing swirl, the strength of the PVC increases at a much larger rate (~5000%) compared to the increase in turbulence intensity (~80%). This is why the flow field is sensitive to turbulence in the low swirl cases but not in cases with a greater degree of swirl ($S > 1.05$).

CONCLUSIONS

In this study, we have characterized the influence of flow field turbulence on the dynamics of the PVC by using the magnitude of jitter in the PVC as a metric for the impact of turbulence on coherent PVC motions. We studied ten swirl numbers, ranging from $S = 0.73 - 1.83$. The flow fields show that the cases with low swirl numbers have a weak and intermittent PVC, whereas the precession is much stronger and more consistent in the higher swirl number cases. The turbulence intensity increases monotonically with swirl number due to the increase in mean

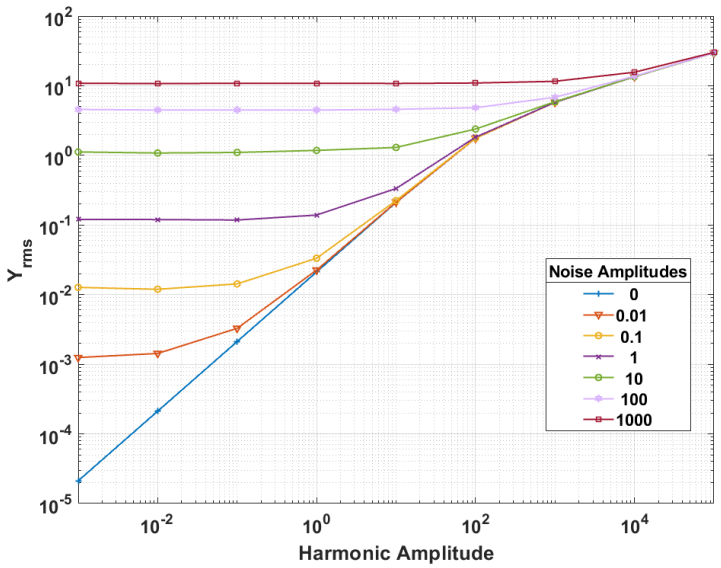

FIGURE 9. RMS of the solution of a van der Pol forced by noise and a harmonic forcing function.

shear in the flow field. Since both the strength of the PVC and the intensity of turbulence are increasing with increasing swirl, the dynamics of their interaction is continually evolving.

In a study of the spatial variation in jitter, we have demonstrated, by using the RMS of the vortex location, that the impact of turbulence on the PVC motion diminishes with increasing swirl despite the increase in turbulence intensity. This transition is observed at swirl number $S = 1.15$. In the frequency domain, the peak is wide at lower swirl numbers, indicating a high degree of temporal jitter. As the swirl number increases, the peak width dips sharply from swirl numbers $S = 0.79 - 1.05$. In the same range, however, spatial jitter still increases, indicating that while the flow field is still sensitive to the influence of turbulence, the coherent motion of the PVC is becoming stronger. For swirl numbers greater than $S = 1.05$, the peak width is nearly constant, indicating that frequency jitter is no longer sensitive to increasing turbulence.

In a parametric analysis of a nonlinear van der Pol oscillator forced by noise and a sinusoidal wavemaker at the oscillator's resonant frequency, we have shown that as the amplitude of the harmonic function increases, the sensitivity of the oscillator response to amplitude of noise decreases. The results indicate that at high values of harmonic amplitude, the behaviour of the oscillator is dictated by the wavemaker and at lower values of harmonic amplitude, the amplitude of noise drives the response. Using the results of the jitter study and analysis of the van der Pol oscillator, we conclude that there are two distinctly observable regimes where the dynamics of the swirling flow field are driven by the flow field turbulence or the coherent motion of the

PVC and the transition between these regimes is strongly linked to the degree of swirl in the system.

ACKNOWLEDGMENT

The authors would like to acknowledge Dr. Santosh Hemchandra and Kiran Manoharan from the India Institute of Science Bangalore for their long-standing collaboration and fruitful feedback on this data. This work was supported by the U.S. National Science Foundation under grant CBET-1749679.

REFERENCES

[1] Harvey, J., 1962. "Some observations of the vortex breakdown phenomenon". *Journal of Fluid Mechanics,* ***14***(4), pp. 585–592.

[2] Benjamin, T. B., 1962. "Theory of the vortex breakdown phenomenon". *Journal of Fluid Mechanics,* ***14***(4), pp. 593–629.

[3] Hall, M., 1972. "Vortex breakdown". *Annual Review of Fluid Mechanics,* ***4***(1), pp. 195–218.

[4] Leibovich, S., 1978. "The structure of vortex breakdown". *Annual Review of Fluid mechanics,* ***10***(1), pp. 221–246.

[5] Lopez, J., 1990. "Axisymmetric vortex breakdown part 1. confined swirling flow". *Journal of Fluid Mechanics,* ***221***, pp. 533–552.

[6] Liang, H., and Maxworthy, T., 2005. "An experimental investigation of swirling jets". *Journal of Fluid Mechanics,* ***525***, p. 115159.

[7] Lucca-Negro, O., and O'Doherty, T., 2001. "Vortex breakdown: a review". *Progress in Energy and Combustion Science,* ***27***(4), pp. 431–481.

[8] Oberleithner, K., Paschereit, C., Seele, R., and Wygnanski, I., 2012. "Formation of turbulent vortex breakdown: intermittency, criticality, and global instability". *AIAA journal,* ***50***(7), pp. 1437–1452.

[9] Gupta, A. K., Lilley, D. G., and Syred, N., 1984. "Swirl flows". *Tunbridge Wells, Kent, England, Abacus Press, 1984, 488 p.*

[10] Ruith, M. R., Chen, P., Meiburg, E., and Maxworthy, T., 2003. "Three-dimensional vortex breakdown in swirling jets and wakes: direct numerical simulation". *Journal of Fluid Mechanics,* ***486***, p. 331378.

[11] Oberleithner, K., Terhaar, S., Rukes, L., and Paschereit, C. O., 2013. "Why nonuniform density suppresses the precessing vortex core". *Journal of Engineering for Gas Turbines and Power,* ***135***(12), p. 121506.

[12] Candel, S., Durox, D., Schuller, T., Bourgouin, J.-F., and Moeck, J. P., 2014. "Dynamics of swirling flames". *Annual Review of Fluid Mechanics,* ***46***, pp. 147–173.

[13] Syred, N., 2006. "A review of oscillation mechanisms and the role of the precessing vortex core (pvc) in swirl combustion systems". *Progress in Energy and Combustion Science,* ***32***(2), pp. 93–161.

[14] Oberleithner, K., Stöhr, M., Im, S. H., Arndt, C. M., and Steinberg, A. M., 2015. "Formation and flame-induced suppression of the precessing vortex core in a swirl combustor: experiments and linear stability analysis". *Combustion and Flame,* ***162***(8), pp. 3100–3114.

[15] Freitag, M., Klein, M., Gregor, M., Nauert, A., Geyer, D., Schneider, C., Dreizler, A., and Janicka, J., 2005. "Mixing analysis of a swirling recirculating flow using dns and experimental data". In Fourth International Symposium on Turbulence and Shear Flow Phenomena, Begel House Inc.

[16] Steinberg, A. M., Boxx, I., Stöhr, M., Carter, C. D., and Meier, W., 2010. "Flow–flame interactions causing acoustically coupled heat release fluctuations in a thermo-acoustically unstable gas turbine model combustor". *Combustion and Flame,* ***157***(12), pp. 2250–2266.

[17] Mathews, B., Hansford, S., and O'Connor, J., 2016. "Impact of swirling flow structure on shear layer vorticity fluctuation mechanisms". In ASME Turbo Expo 2016: Turbomachinery Technical Conference and Exposition, American Society of Mechanical Engineers, pp. V04AT04A026–V04AT04A026.

[18] Frederick, M., Manoharan, K., Dudash, J., Brubaker, B., Hemchandra, S., and O'Connor, J., 2018. "Impact of precessing vortex core dynamics on shear layer response in a swirling jet". *Journal of Engineering for Gas Turbines and Power,* ***140***(6), p. 061503.

[19] Hussain, A. K. M. F., and Reynolds, W. C., 1970. "The mechanics of an organized wave in turbulent shear flow". *Journal of Fluid Mechanics,* ***41***(2), pp. 241–258.

[20] Midgley, K., Spencer, A., and McGuirk, J. J., 2005. "Unsteady flow structures in radial swirler fed fuel injectors". *Journal of Engineering for Gas Turbines and Power,* ***127***(4), pp. 755–764.

[21] Liou, T., and Santavicca, D., 1985. "Cycle resolved ldv measurements in a motored ic engine". *Journal of Fluids Engineering,* ***107***(2), pp. 232–240.

[22] Brereton, G., and Kodal, A., 1992. "A frequency-domain filtering technique for triple decomposition of unsteady turbulent flow". *Journal of Fluids Engineering,* ***114***(1), pp. 45–51.

[23] Oberleithner, K., Sieber, M., Nayeri, C., Paschereit, C., Petz, C., Hege, H.-C., Noack, B., and Wygnanski, I., 2011. "Three-dimensional coherent structures in a swirling jet undergoing vortex breakdown: stability analysis and empirical mode construction". *Journal of Fluid Mechanics,* ***679***, pp. 383–414.

[24] Citriniti, J., and George, W. K., 2000. "Reconstruction of the global velocity field in the axisymmetric mixing layer utilizing the proper orthogonal decomposition". *Journal of Fluid Mechanics,* ***418***, pp. 137–166.

[25] Graftieaux, L., Michard, M., and Grosjean, N., 2001. "Combining piv, pod and vortex identification algorithms for the study of unsteady turbulent swirling flows". *Measurement Science and technology,* ***12***(9), p. 1422.

[26] Towne, A., Schmidt, O. T., and Colonius, T., 2018. "Spectral proper orthogonal decomposition and its relationship to dynamic mode decomposition and resolvent analysis". *Journal of Fluid Mechanics,* ***847***, pp. 821–867.

[27] Terhaar, S., Ćosić, B., Paschereit, C., and Oberleithner, K., 2016. "Suppression and excitation of the precessing vortex core by acoustic velocity fluctuations: An experimental and analytical study". *Combustion and Flame,* ***172***, pp. 234–251.

[28] Tammisola, O., and Juniper, M. P., 2016. "Coherent structures in a swirl injector at re = 4800 by nonlinear simulations and linear global modes". *Journal of Fluid Mechanics,* ***792***, p. 620657.

[29] Shanbhogue, S. J., Seelhorst, M., and Lieuwen, T., 2009. "Vortex phase-jitter in acoustically excited bluff body flames". *International Journal of Spray and Combustion Dynamics,* ***1***(3), pp. 365–387.

[30] Hussain, A. F., and Hayakawa, M., 1987. "Eduction of large-scale organized structures in a turbulent plane wake". *Journal of Fluid Mechanics,* ***180***, pp. 193–229.

[31] Lefebvre, A. H., 1998. *Gas Turbine Combustion*. CRC press.

[32] Schmid, P. J., 2010. "Dynamic mode decomposition of numerical and experimental data". *Journal of Fluid Mechanics,* ***656***, p. 528.

[33] Manoharan, K., Hansford, S., O'Connor, J., and Hemchandra, S., 2015. "Instability mechanism in a swirl flow combustor: precession of vortex core and influence of density gradient". In ASME Turbo Expo 2015: Turbine Technical Conference and Exposition, American Society of Mechanical Engineers, pp. V04AT04A073–V04AT04A073.

[34] van der Pol, B., 1926. "Lxxxviii. on relaxation-oscillations". *The London, Edinburgh, and Dublin Philosophical Magazine and Journal of Science,* ***2***(11), pp. 978–992.